ADVANCED HEALTHCARE MATERIALS
www.advhealthmat.de

Bleeding the Excited State Energy to the Utmost: Single-Molecule Iridium Complexes for In Vivo Dual Photodynamic and Photothermal Therapy by an Infrared Low-Power Laser

*Shi-Jie Tang, Qing-Fang Li, Meng-Fan Wang, Rong Yang, Li-Zhen Zeng, Xue-Lian Li, Rui-Dong Wang, Hongbin Zhang, Xiaoxia Ren, Dan Zhang, and Feng Gao**

A series of cyclometalated Ir(III) complexes with morpholine and piperazine groups are designed as dual photosensitizers and photothermal agents for more efficient antitumor phototherapy via infrared low-power laser. Their ground and excited state properties, as well as the structural effect on their photophysical and biological properties, are investigated by spectroscopic, electrochemical, and quantum chemical theoretical calculations. They target mitochondria in human melanoma tumor cells and trigger apoptosis related to mitochondrial dysfunction upon irradiation. The Ir(III) complexes, particularly Ir6, demonstrate high phototherapy indexes to melanoma tumor cells and a manifest photothermal effect. Ir6, with minimal hepato-/nephrotoxicity in vitro, significantly inhibits the growth of melanoma tumors in vivo under 808 nm laser irradiation by dual photodynamic therapy and photothermal therapy and can be efficiently eliminated from the body. These results may contribute to the development of highly efficient phototherapeutic drugs for large, deeply buried solid tumors.

1. Introduction

Photodynamic therapy (PDT) is a promising cancer treatment that involves the generation of reactive oxygen species (ROS) by photosensitizers (PSs) upon light irradiation, resulting in noninvasive tumor cell death.[1] PDT is partially dependent on oxygen availability. Tumors, particularly big solid tumors, have a hypoxic environment that significantly limits the efficacy of PDT due to rapid cell proliferation, limited vascular development, and uneven distribution. The combination of PDT with one or more other novel therapeutics, such as photothermal therapy (PTT), photoacoustic therapy (PAT), photochemotherapy (PCT), and immunogenic cell death (ICD), can integrate their respective benefits, significantly improve treatment efficacy, and reduce the dosage of therapeutic agents.[2]

Oxygen-independent PTT can be simply performed in conjunction with PDT, inducing thermal ablation of tumors without the need for additional equipment or reagents.[3] Nevertheless, PSs based on monomolecular metal complexes, such as $[Ru(bpy)_3]^{2+}$ and $[Ir(ppy)_2bpy]^{2+}$, have virtually no photothermal conversion (PTC) capability. Therefore, the PTC effect is not an inherent feature of metal complexes, and specific structural modifications are required for the development of photothermal agents (PTAs) based on metal complexes. The reported metal complexes that can be employed for dual PDT/PTT therapy comprise ligands with aggregation tendencies and are preprepared in aggregation states, such as micelles, solid nanoparticles (NPs), and so on.[4] Despite existing concerns regarding the safety of NPs, the manufacture of such complex aggregates, the variety of materials employed, and the size heterogeneity of individual particles make their future pharmaceutical work extremely challenging. The encapsulation of multiple ingredients in the carrier or their conjugation with the carrier generally causes an excess of parenteral excipients and low active-ingredient loading. Therefore, it is really necessary to have a single active component, which can eliminate the tedious procedures as well as improve the bioavailability of synergistic therapy agents.[3,5]

S.-J. Tang, Q.-F. Li, M.-F. Wang, R. Yang, L.-Z. Zeng, X.-L. Li, R.-D. Wang, H. Zhang, F. Gao
Key Laboratory of Medicinal Chemistry for Natural Resource
Ministry of Education
Yunnan Provincial Center for Research & Development of Natural Products
School of Pharmacy
Yunnan University
Kunming 650500, P. R. China
E-mail: gaofeng@ynu.edu.cn

X. Ren
Animal Research and Resource Center
School of Life Sciences
Yunnan University
Kunming 650091, P. R. China

D. Zhang
First Affiliated Hospital of Kunming Medical University
Kunming 650032, P. R. China

The ORCID identification number(s) for the author(s) of this article can be found under https://doi.org/10.1002/adhm.202301227

DOI: 10.1002/adhm.202301227

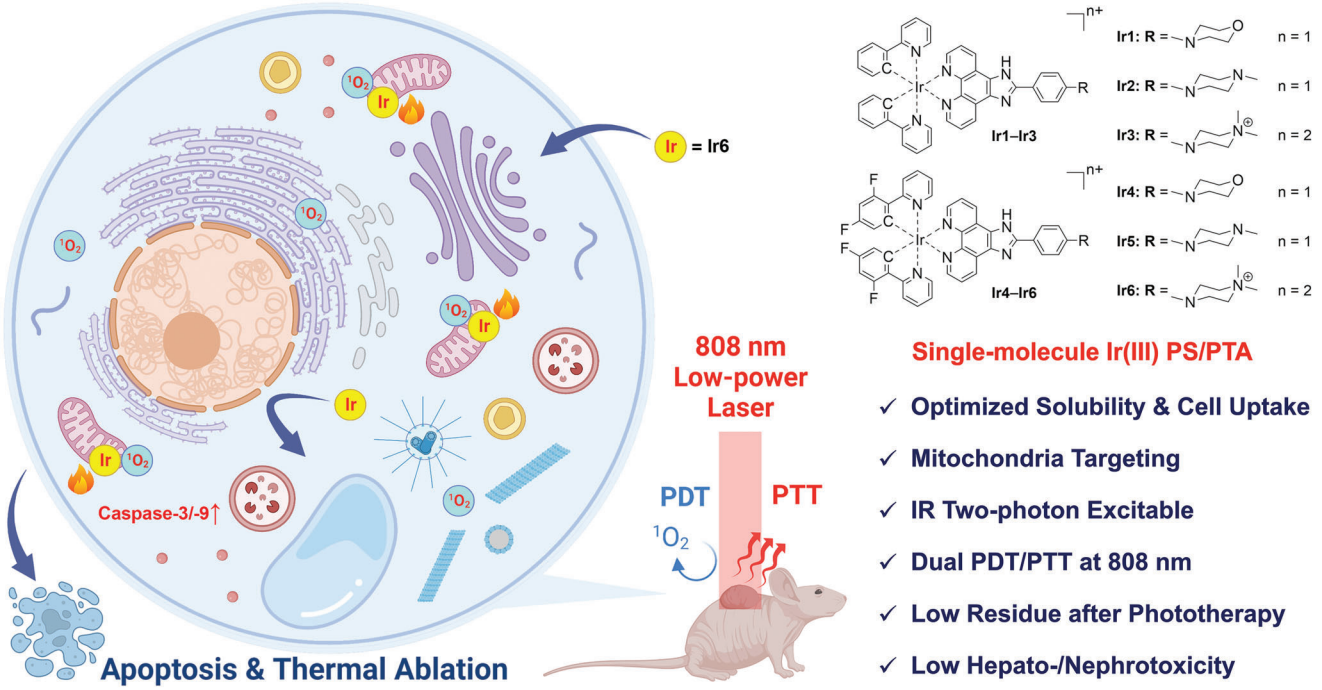

Figure 1. Structures and characteristics of cyclometalated Ir(III) complexes **Ir1–6** designed in this study as IR two-photon excitable single-molecule photosensitizers/photothermal agents (PSs/PTAs) for in vivo antitumor photodynamic/photothermal therapy (PDT/PTT).

To this end, we have realized the single-molecule antitumor dinuclear Ru(II) complexes for dual PDT/PTT in vivo by modulating triple excited states (^{3}ESs) with a lowered energy level for efficient energy transfer to oxygen and a large rotatable substituent group for convenient nonradiative (exothermic) decay.[6] Intriguingly, their dinuclear Os(II) counterparts have ^{3}ESs with even lower energy, rendering practically all of their ES energy decaying via heat release, resulting in an enhancement in PTT activity and an elimination of PDT activity.[7] The balance of ES energy in three aspects, namely, radiation decay (luminescence), nonradiation decay (heat release), and energy transfer with oxygen, may be crucial to the therapeutic mechanism and efficacy of a PS or/and PTA.

Cyclometalated Ir(III) complexes are widely used as luminescent materials and antitumor PSs due to their extended ^{3}ES lifetime and high quantum yield of both emission and $^1O_2$ production.[8] In this study, by introducing vibrational heterocyclic groups onto a pip-type ligand and rotatable methyl substituents, we designed a series of single-molecule Ir(III) complexes as infrared (IR) two-photon absorption (TPA) PSs with remarkable photothermal conversion efficiency (PCE) (**Figure 1**). Using an 808 nm IR low-power laser (LPL, 100 mW cm^{-2}), the most effective **Ir6** was successfully applied in the dual PDT/PTT for malignant melanoma in mice. These findings may contribute to the development of highly efficient phototherapeutic drugs for large, deeply buried solid tumors in hypoxic environments.

Residues in the body and cumulative hepatorenal toxicity are key safety concerns for metal-containing drugs.[9] During the in vivo investigation, we attempted to identify the quantities of iridium persisting in various organs of mice after phototherapy. After intravenous administration, **Ir6** was swiftly removed from the bodies of mice within 14 d, with just trace amounts remaining in the liver, kidneys, and tumors. Further research revealed that **Ir6** has negligible hepatorenal toxicity without IR irradiation, increasing confidence in its safety for further pharmacological study.

2. Results and Discussion

2.1. Photophysical Properties

The UV–vis absorption spectra of **Ir1–6** in aqueous solution at 25 °C were recorded (**Figure 2**a). The band maxima (λ_{abs}) and molar extinction coefficients (ϵ) were summarized in **Table 1**. The absorbance follows the Beer–Lambert law in the concentration range of 1–50 × 10^{-6} M, suggesting the absence of ground state aggregation in this tested concentration range. The spectra of **Ir1–6** are comprised of three main absorption bands. With the assistants of time-dependent density functional theory (TDDFT) calculations (Figure 2b; Figures S1–S6 and Table S1, Supporting Information), the weak band extending to 410–467 nm is attributed to the spin-allowed intraligand (^{1}IL), or called ligand-centered (^{1}LC), π–π^* transitions on the N^N ligands, whereas the two strong bands locate below 350 nm originate from the ligand-to-ligand charge-transfer (^{1}LLCT), metal-to-ligand charge-transfer (^{1}MLCT), ^{1}IL transitions on the C^N ligands, and their respective combinations.

The steady state emission spectra of **Ir1–6** were recorded in aqueous solution at 25 °C, and the emission wavelengths (λ_{em}) and quantum yields (Φ) were summarized in Table 1. **Ir1–3** exhibit consistent emission wavelengths, while those of **Ir4–6** are quite different. From the theoretical results by TDDFT

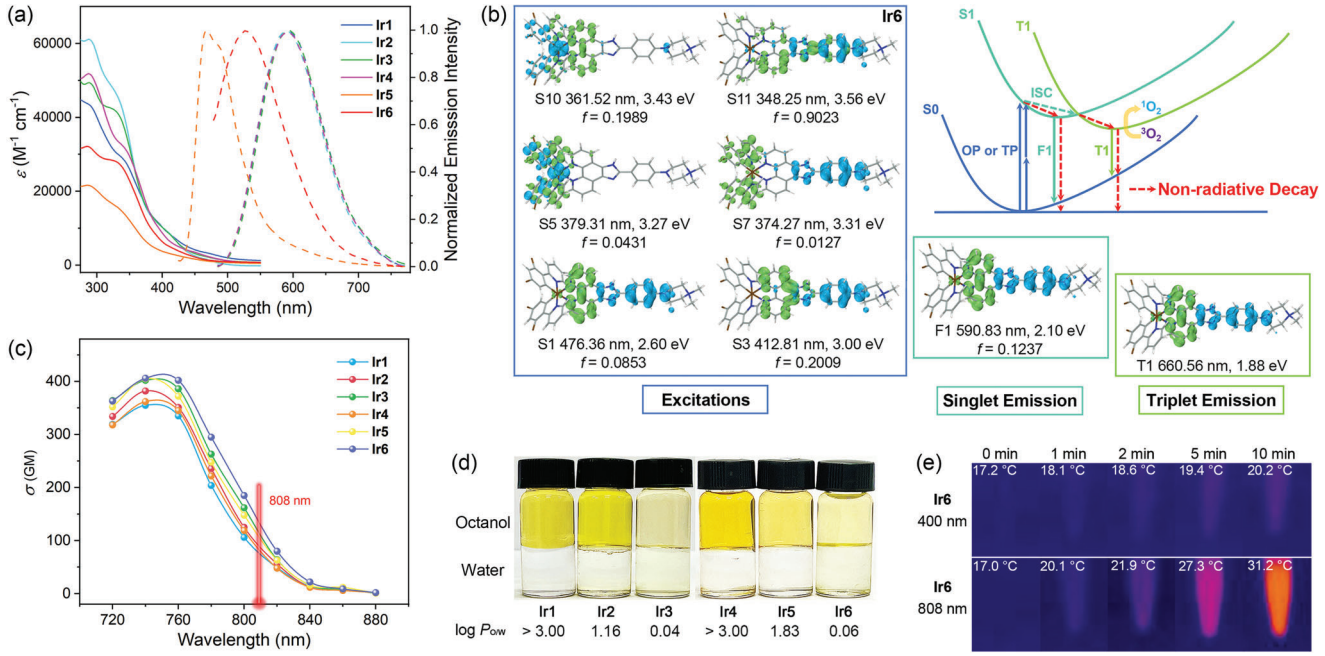

Figure 2. Photophysical, photochemical, and bioactivity-related properties of **Ir1–6**. a) Absorption (solid) and normalized emission spectra (dashed) in aqueous solution. b) Real space representation of hole (blue) and electron (green) distributions of **Ir6** for the main excited state transitions responsible for excitation (Sn), first singlet emission (F1), and triplet emission (T1). Excitation wavelength (nm), excitation energy (eV), and oscillator strength (*f*) for each hole-to-electron transition are presented (B3LYP/Lanl2DZ, CPCM). The simplified Jablonski diagraph describes the energy transfer and main nonradiative decay (heat release) pathways. c) TPASCs (σ) of **Ir1–6** in the range of 720–880 nm. d) The distributions of **Ir1–6** between *n*-octanol and aqueous phases. e) Representative thermal images of **Ir6** in aqueous solution (100×10^{-6} M) irradiated by 400 nm LED (50 mW cm^{-2}) and 808 nm LPL (100 mW cm^{-2}) for 1, 2, 5, and 10 min.

Table 1. Photophysical and electrochemistry data for **Ir1–6**.

Complex	λ_{abs} [a] [nm] (ε /10^4 M^{-1} cm^{-1})	λ_{em} [a] [nm]	Φ [a]	τ [a] [ns]	E_{ox} [b] [V]	E_{red} [b] [V]
Ir1	290 (4.32), 344 (2.79), 467 (0.33)	593	0.104	8.02	0.52, 0.79	−1.24, −1.58, −2.10
Ir2	287 (6.11), 336 (4.39), 410 (0.88)	588	0.085	34.7	0.70, 0.90	−1.26, −1.67, −2.08
Ir3	289 (4.95), 330 (4.16), 411 (0.85)	593	0.050	52.4	0.68, 0.86	−1.30, −1.73, −2.00
Ir4	287 (5.19), 346 (3.08), 447 (0.36)	593	0.085	4.29	0.52, 0.84	−1.03, −1.42, −2.03
Ir5	285 (2.17), 339 (1.45), 428 (0.24)	489	0.066	1.71	0.70, 0.94	−1.24, −1.34, −1.99
Ir6	286 (3.22), 329 (2.80), 431 (0.33)	527	0.022	13.8	0.71, 0.86	−1.14, −1.48, −2.01

[a] In air-saturated aqueous solution at 25 °C; [b] In air-saturated anhydrous acetonitrile at 25°C.

(Figure 2b; Figures S5 and S6, Supporting Information), the emissions of **Ir4–6**, from either singlet or triplet states, are produced by radiation transitions of the IL excited states on the N^N ligand. This transition involves the introduced heterocycles, which have different electronic effects and may give rise to the wide variations in λ_{em}. For **Ir1–3**, however, there is a singlet emission state with a lower energy level and oscillator strength (*f*) below the heterocycle-involved state (Figures S2–S4, Supporting Information). This state has the nature of ^{1}LLCT from the C^N ligands to the phenanthroline part of the N^N ligand and ^{1}MLCT from Ir(III) to the same destination. Therefore, **Ir1–3** show little difference in emission energy since their emission is not affected by the heterocycles.

The luminescence lifetime (τ) of **Ir1–6** were further examined in aqueous solution at 25 °C. From the rather short lifetimes (in nanoseconds), these emissions are credited to fluorescence from ^{1}IL rather than phosphorescence from ^{3}IL, although they have quite identical configurations. Since no phosphorescence lifetime is detected in the microsecond or second window, we postulate that **Ir1–6** have a dark (nonradiative) ^{3}IL state. Phosphorescence is mainly manifested under conditions where vibrational relaxation is limited, such as low temperature, solid state, and so on. Under physiological conditions (>25 °C and in the mobile single-molecule state), energy transfer (generating $^1O_2$ for PDT) and nonradiative decay (releasing heat for PTT) will become the main dissipation pathways of the ^{3}IL state energy of iridium complexes. The same finding holds true for BODIPY-Ir, where the difference in energy level between the lowest singlet and triplet excited states (F1 and T1) is as low as **Ir1–6**.[4b] Such a dark triplet state has been regarded as advantageous for preventing excessive

loss of excited state energy and maximizing its usage in PDT and PTT.

2.2. Electrochemistry

According to previous studies, the oxidation potential of a PS is important for its ROS generation.[4c,10] Thus, the redox properties of **Ir1–6** were evaluated in acetonitrile (MeCN) by cyclic voltammetry using the Fc^+/Fc couple as the internal standard. Three irreversible reduction processes were observed for **Ir1–6**, corresponding to the reductions of one N^N and two C^N ligands, as seen for similar Ir(III) complexes.[11] Two oxidation processes were discovered, one irreversible and one reversible. The reduction and oxidation potentials (E_{red} and E_{ox}) were listed in Table 1. Since the HOMOs and LUMOs of **Ir1–6** were both populated on the N^N ligand, the first oxidation was expected to occur on the N^N ligand, while the second oxidation was attributed to Ir(IV)/Ir(III) oxidation owing to the Ir(III) centered HOMO-1 and the typical values of E_{ox} for Ir(IV)/Ir(III) in cyclometalated Ir(III) complexes (0.8–1.0 V). This provides more evidence that ligand-centered HOMO and low-energy IL excited states readily participate in the electronic/energy transfer of PS.

2.3. Two-Photon Absorption

Excitation at 405 nm enabled the aforementioned research on excited state characteristics. Due to its low tissue penetration, visible light with such a short wavelength has limited applications in phototherapy. In addition, in the absence of any PS, this high-energy irradiation can generate biological damage such as DNA photocleavage, cell death, eye and skin damage, etc. Benefiting from their exceptional TPA capabilities, Ir(III)-PSs can have their excitation wavelength nearly doubled to 800 nm. Therefore, the TPA capacity and excitability of Ir(III)-PSs are crucial for their application in phototherapy. The TPA cross-sections (σ) of **Ir1–6** have been determined by two-photon (TP) excited fluorescence. All Ir(III) complexes produce distinct fluorescence signals in the range of 720–840 nm upon TP excitation (Figure 2c). TPA maxima are detected between 740 and 760 nm with remarkable σ values between 357 and 415 GM. The σ values at 808 nm (σ_{808}) are 79–142 GM, which are higher than similar mononuclear Ir(III)[11b,12] and Ru(II)[13] complexes at around 800 nm but lower than certain dinuclear Ir(III),[14] Ru(II),[6,15] and Os(II)[7] complexes. Therefore, **Ir1–6** can be expected to be potent PSs that can be excited by the 808 nm LPL.

2.4. Singlet Oxygen Quantum Yield

The $^1O_2$ generation efficiency of a PS plays an essential role in its photocytotoxicity. The $^1O_2$ quantum yields (Φ_Δ) of **Ir1–6** in aqueous solution have been quantified by a $^1O_2$ trapping probe, 9,10-anthracenediyl-bis(methylene)dimalonic acid (ABDA). As depicted in Figures S7 and S8 (Supporting Information), the absorbance of Ir(III) complex-containing ABDA decreased rapidly under irradiation with 400 nm LED (50 mW cm^{-2}) and 808 nm LPL (100 mW cm^{-2}), indicating the generation of $^1O_2$. Using a photon counting technic (detailed in the Supporting Information), the $^1O_2$ quantum yields under 400 and 808 nm excitation ($\Phi_{\Delta400}$ and $\Phi_{\Delta808}$, **Table 2**) could be calculated by taking into account the difference in photon numbers of excitation lights of various wavelengths. **Ir4–6** with fppy C^N ligands showed higher Φ_Δ values than **Ir1–3** with ppy C^N ligands and the same N^N ligand. **Ir1** and **Ir4** containing bismethylpiperazine (BMP) exhibited higher Φ_Δ than **Ir2** and **Ir5** bearing monomethylpiperazine (MMP), followed by **Ir3** and **Ir6** with morpholine (MP).

Table 2. Bioactivity-related properties of **Ir1–6**.

Compound	σ_{808} [a] [GM]	$\Phi_{\Delta400}$ [b]	$\Phi_{\Delta808}$ [b]	η_{808} [c] [%]	log $P_{O/W}$ [d]
Ir1	79	0.62	0.026	17.1	>3.00
Ir2	94	0.78	0.063	17.6	1.16
Ir3	120	0.82	0.078	17.2	0.04
Ir4	87	0.74	0.031	17.0	>3.00
Ir5	112	0.82	0.070	17.9	1.83
Ir6	142	0.96	0.110	18.0	0.06

[a] Two-photon absorption cross-section at 808 nm (1 GM = 10^{-50} cm^4 s $photon^{-1}$); [b] Singlet oxygen quantum yield upon 400 nm LED (50 mW cm^{-2}) and 808 nm LPL (100 mW cm^{-2}) irradiation in aqueous solution; [c] Photothermal conversion efficiency at 808 nm; [d] Oil/water partition coefficient (standard deviation < 5%).

The $\Phi_{\Delta400}$ value is 0.96 for **Ir6** in aqueous solution, indicating a high efficiency with which the energy of the excited state is transferred to $^1O_2$ through ^{3}IL during OP excitation. In cases of TP excitation, $\Phi_{\Delta808}$ values are apparently decreased. First, this is due to the TPA efficiency barrier, which means that not all 808 nm photons can be simultaneously absorbed in pairs and perform the excitation function. Second, the use of a low-energy infrared laser further reduces excitation efficiency, albeit increasing the feasibility and safety of TP phototherapy. Finally, the upper limit of $\Phi_{\Delta808}$ should be 0.5, according to the definition of quantum yield, since TP excitation requires the absorption of two photons by the PS to produce one $^1O_2$. The $\Phi_{\Delta808}$ value of **Ir1–6** are quite remarkable, in comparison to $[Ru(bpy)_3]^{2+}$ (0.006) and a serious of dinuclear Ru(II) PSs (0.020–0.156),[6] under identical experimental conditions. The negative correlation between Φ_Δ and Φ is another notable observation. This might imply that radiative decay and energy transfer have a compensatory relationship. **Ir6**, with the lowest fluorescence emission intensity and the highest $\Phi_{\Delta808}$, may become the most promising PS of the series.

2.5. Photothermal Conversion Efficiency

Given the unique advantages of solid materials and IR in photothermal conversion (PTC), some Ir(III) complex-containing nanoparticles (NPs) and aggregates exhibit excellent PCE at 808 nm, despite the fact that their Ir(III) components lack PTC capacity as monomers.[4b,c,16] Appropriate structural modification and the inclusion of rotatable substituent groups may significantly enhance the PCE of non-emitting BODIPY-type photothermal agent (PTA) and BODIPY-encapsulated NP to above 88%.[16b,c,17] Undoubtedly, finding out if this strategy may be employed as well for constructing single-molecule Ir(III)-based dual TPA-PS/PTA is a worthy endeavor.

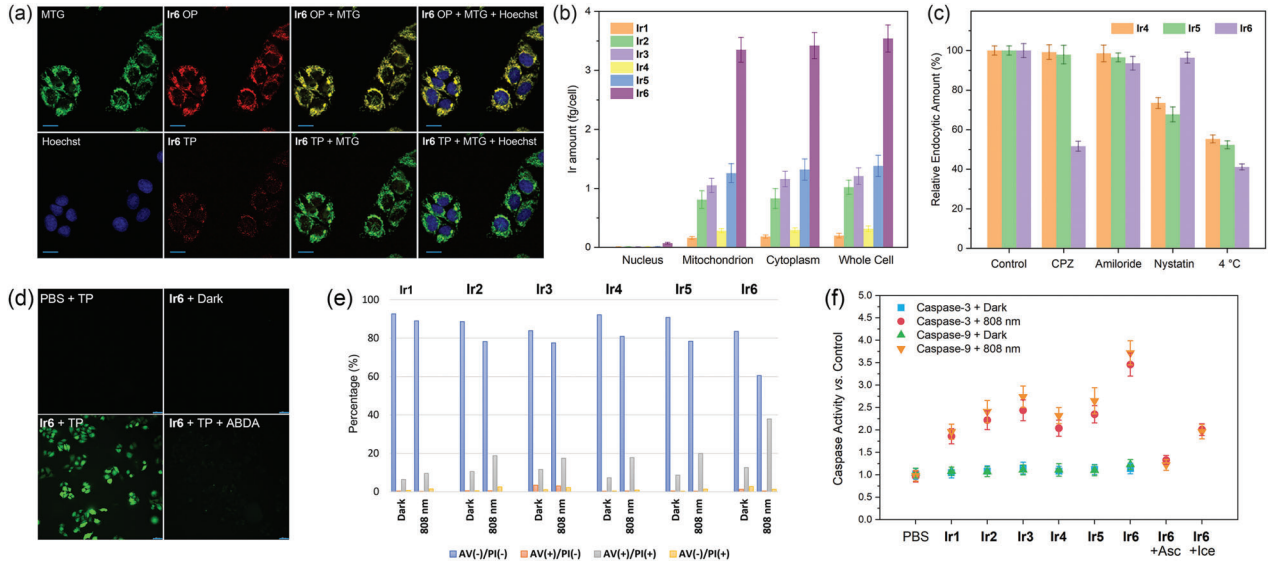

Figure 3. Cellular localization, uptake, photoinduced apoptosis, and mechanism of Ir(III) complexes. a) Subcellular colocalization of **Ir6** with MitoTracker Green (MTG) and Hoechst 33324 (Hoechst) in A375 human melanoma cells by confocal laser scanning microscopy (CLSM) upon one-photon (OP, 405 nm) and two-photon (TP, 808 nm) excitations (scale bar: 20 μm). b) The distribution of iridium for **Ir1**–**6** in various regions of A375 cells as determined by inductively coupled plasma mass spectrometry (ICP-MS). Data represent the mean ± SD ($n = 3$). c) Relative uptake amount of **Ir4**–**6** in the presence of endocytic inhibitor chlorpromazine (CPZ, 10.0 μg mL^{-1}), amiloride (100.0 μg mL^{-1}), or nystatin (50.0 μg mL^{-1}) at 37 °C or without inhibitor at 4 °C. Data represent the mean ± SD ($n = 3$). d) DCF-indicated intracellular $^1O_2$ generation by **Ir6** upon TP excitations (scale bar: 50 μm) and its suppression by $^1O_2$ scavenger ABDA (100 × 10^{-6} M). e) Flow cytometry detection (stained with Annexin V-FITC and PI) of photoinduced apoptosis in A375 cells induced by Ir(III) complexes in the absence and presence of 808 nm LPL (100 mW cm^{-2}) irradiation. f) Caspase-3 and -9 activity in A375 cells after treatment with PBS (control) and Ir(III) complexes in the dark and under 808 nm LPL (100 mW cm^{-2}) irradiation. Data represent the mean ± SD ($n = 3$).

The PCEs of **Ir1**–**6** were measured in aqueous solution. When exposed to 808 nm LPL, the temperatures of **Ir1**–**6** solution (100 × 10^{-6} M) steadily increased with $\Delta T = 13.3$–14.2 °C (Figure 2e and Figure S9, Supporting Information). The amplitude of the temperature increase has a strong concentration dependence. After four cycles of heating/cooling, the performance has remained largely unaltered. The PCEs of **Ir1**–**6** at 808 nm (η_{808}, Table 2) show no discernible individual differences (17.0%–18.0%), indicating that the complexes release heat primarily through the rich and diverse vibration modes of the flexible and mobile six-membered ring, while the rotation of the methyl substituents may not play a significant role. In contrast, analogues of **Ir1**–**6** containing rigid conjugated ligands have no PTC activity under the same conditions,[11b] highlighting the crucial role of the six-membered ring in heat release. The PCEs of **Ir1**–**6** are lower than those of the self-assembled aggregates of IrDAD (27.5%, 808 nm laser, 700 mW cm^{-2}), in which aggregation played an essential part in the PTC.[4c] Despite having a 50% greater PCE than **Ir1**–**6**, IrDAD has lost the ability to generate $^1O_2$ in a single-molecule state. **Ir1**–**6** are therefore the only example of single-molecule Ir(III) complexes with both the capacity to produce $^1O_2$ and the PTC activity at 808 nm, supporting their application as dual PDT/PTT reagents.

2.6. Lipophilicity and Solubility

Figure 2d and Figure S10 (Supporting Information) show the lipophilicity (log $P_{O/W}$ values) of **Ir1**–**6**. The complexes displayed substituent-dependent lipophilicity (Table 2). **Ir1** and **Ir4** with MP group exhibited significant log $P_{O/W}$ values greater than 3.0 and extremely poor solubilities in aqueous solution (20 × 10^{-6} M, 5% DMSO), which may be disadvantaged to their drug utilization. **Ir2** and **Ir5** with MMP group showed moderate lipophilicity and better solubility (50 × 10^{-6} M, 5% DMSO). **Ir3** and **Ir6** with BMP group had an optimum hydrophilic and hydrophobic balance and quite high solubility (>100 × 10^{-6} M without DMSO), which is beneficial in the process of pharmaceutical application, such as a balanced volume of distribution and the potential for good absorption and bioavailability.[18]

2.7. Subcellular Localization and Cell Uptake

The effectiveness of PDT and PTT depends heavily on the cell uptake and intracellular localization of PSs and PTAs. As shown in **Figure 3**a and Figure S15 (Supporting Information), all Ir(III) complexes showed red luminescence within cells. For hydrophobic **Ir1**, **Ir2**, **Ir4**, and **Ir5**, the complex precipitated around or inside the cell at concentrations that did not reach their saturated solubility. This suggests that some parts of the cell can enrich and locally supersaturate the complex. For amphiphilic Ir3 and Ir6, no precipitation was generated. The signals of **Ir3** and **Ir6** matched well with the mitochondrial dye MTG, suggesting that they target mitochondria in cells.

The cell uptake and pathway of **Ir1**–**6** were further investigated. ICP-MS findings suggest that at the same concentration of complex, **Ir6** was taken up by cells the most (Figure 3b). Its

Table 3. In vitro cytotoxicities (IC_{50}, μM) of Ir(III) complexes and cisplatin against A375 cell lines under various conditions.

Compound	Dark[a]	TP[b]	PI[c]	TP+Asc[d]	TP+Ice[e]	TP+Asc+Ice[f]
Ir1	>20	14.2 ± 1.1	>1.41	>20	>20	>20
Ir2	>50	4.12 ± 0.27	>12.1	44.2 ± 5.6	38.4 ± 4.9	>50
Ir3	134 ± 11	3.10 ± 0.21	43.3	76.0 ± 3.1	22.5 ± 2.8	115 ± 10
Ir4	>20	17.8 ± 1.3	>1.12	>20	>20	>20
Ir5	>50	11.3 ± 1.0	>4.42	>50	>50	>50
Ir6	113 ± 10	0.347 ± 0.022	325	58.5 ± 4.9	13.6 ± 0.50	98.6 ± 8.1
Cisplatin	1.62 ± 0.12	1.36 ± 0.11	1.19	1.39 ± 0.11	1.42 ± 0.12	1.53 ± 0.13

[a] Under dark condition; [b] Upon two-photon (TP) excitation by an 808 nm LPL (100 mW cm^{-2}, light dose = 30.0 J cm^{-2}); [c] Phototherapy indexes (PIs) under TP excitation; [d] TP excitation in the presence of ascorbic acid (Asc, 1.0×10^{-3} M); [e] TP excitation in an ice bath; [f] TP excitation in an ice bath with Asc (1.0×10^{-3} M). Data represent the mean ± SD ($n = 6$).

distribution in mitochondria accounted for up to 95% of the total cellular uptake. **Ir6** showed decreased uptake in the presence of the clathrin inhibitor chlorpromazine (CPZ) and at 4°C, indicating clathrin-mediated and energy-dependent pathways. The uptake of **Ir4** and **Ir5** was inhibited by nystatin and at 4 °C, indicating that they entered the cell via caveolae-mediated and energy-dependent pathways. It is interesting that slight modifications in ligand structures lead to different endocytic pathways of Ir(III) complexes. **Ir6**, which can penetrate cells effectively, may perform better in antitumor phototherapy.

2.8. Intracellular $^1O_2$ Generation

Intracellular $^1O_2$ generation of **Ir6** was analyzed using the ROS detector DCFH-DA (2′,7′-dichlorodihydrofluorescein diacetate, Figure 3d). No ROS was identified in the absence of **Ir6** (PBS+TP) or in the dark (**Ir6**+Dark). Strong DCF (dichlorofluorescein) signals have been observed in the presence of **Ir6** upon TP excitation (**Ir6**+TP), showing efficient production of ROS. The almost complete suppression of DCH fluorescence upon addition of the $^1O_2$ scavenger ABDA (**Ir6**+TP+ABDA) indicates that $^1O_2$ is the major ROS generated by **Ir6**.

2.9. In Vitro Cytotoxicity

Under dark conditions, **Ir3** and **Ir6** displayed fairly low toxicity ($IC_{50} > 100 \times 10^{-6}$ M) to A375 cells, as determined by the CCK-8 assay (**Table 3**). **Ir1**, **Ir2**, **Ir4**, and **Ir5** did not inhibit cell viability at their respective limits of solubility (20 or 50 μM× 10^{-6} M). Since 400 nm irradiation directly induces cell damage, only 808 nm LPL irradiation was used to assess photocytotoxicity. **Ir1**–**Ir6** exhibited notable photocytotoxicities. **Ir6** achieved a phototherapy index (PI) of 325, ranking it among the most effective phototherapeutic molecules and materials recorded to date. As a chemotherapeutic drug, cisplatin showed no significant change in toxicity (PI = 1.15–1.62) under either dark or irradiation conditions. To reveal the relative contributions of PDT and PTT to the photocytotoxicities of **Ir1**–**Ir6**, cytotoxicities were examined in the presence of a ROS scavenger, ascorbic acid (Asc, 1.0×10^{-3} M), or in an ice bath.[4b] Due to the elimination of PDT and PTT activity, the addition of Asc and treatment with an ice bath during irradiation decreased photocytotoxicity for Ir(III) complexes. Simultaneous inhibition of PDT and PTT effects led to an almost complete loss of photocytotoxicity. Hence, their strong photocytotoxicity results from a combined PDT/PTT effect. In addition, the toxicity of PDT or PTT alone was significantly lower than that of dual PDT/PTT, indicating a synergistic effect between the two mechanisms. **Ir6** thus functions as a powerful dual PS/PTA with minimal cytotoxicity in the dark.

2.10. Apoptosis Assay and Caspase Activation

Photogenerated $^1O_2$ triggers the mitochondrial pathway of apoptosis in melanoma cells.[19] Apoptosis of A375 cell lines induced by **Ir1**–**Ir6** during dual PDT/PTT were investigated by Annexin V-FITC/propidium iodide (PI) staining (Figure S13, Supporting Information). The data for each quadrant were illustrated in Figure 3e. Under dark conditions, A375 cells treated with Ir(III) complex showed patterns quite comparable to those of blank cells. Upon irradiation, the late apoptotic fractions of Ir(III) complex-treated cells increased, particularly for **Ir6**, suggesting that they may promote apoptosis in tumor cells. In the apoptotic process, caspase-9 propagates a cascade of further caspase processing events by directly cleaving and activating caspase-3 and caspase-7 to execute cell death.[20] Caspase-3 and -9 activity was measured in A375 cells treated with Ir(III) complexes (Figure 3f). All complexes exhibited no caspase-3 or -9 activation under dark conditions. With 808 nm LPL irradiation, both caspase-3 and -9 activity rose substantially. These findings demonstrate that Ir(III) complexes initiate a photo-dependent apoptosis mechanism.

Although laser-irradiated "hot" NPs stimulate the intrinsic/mitochondrial pathway of apoptosis,[21] no single-molecule has been identified to trigger apoptosis by PTC. The caspase activity of **Ir6**-treated A375 cells decreased greatly in the presence of Asc (Figure 3f), due to the clearance of $^1O_2$. Nonetheless, the activities remained higher than 1, suggesting that the apoptosis was not entirely dependent on $^1O_2$. In addition, when the cells were irradiated in an ice bath, caspase activity also decreased. Therefore, besides $^1O_2$, the heat released by irradiated **Ir6** also contributed to the activation of caspase and cell apoptosis. This favorable characteristic offers crucial support for the development of **Ir6** as a highly effective dual PDT/PTT reagent.

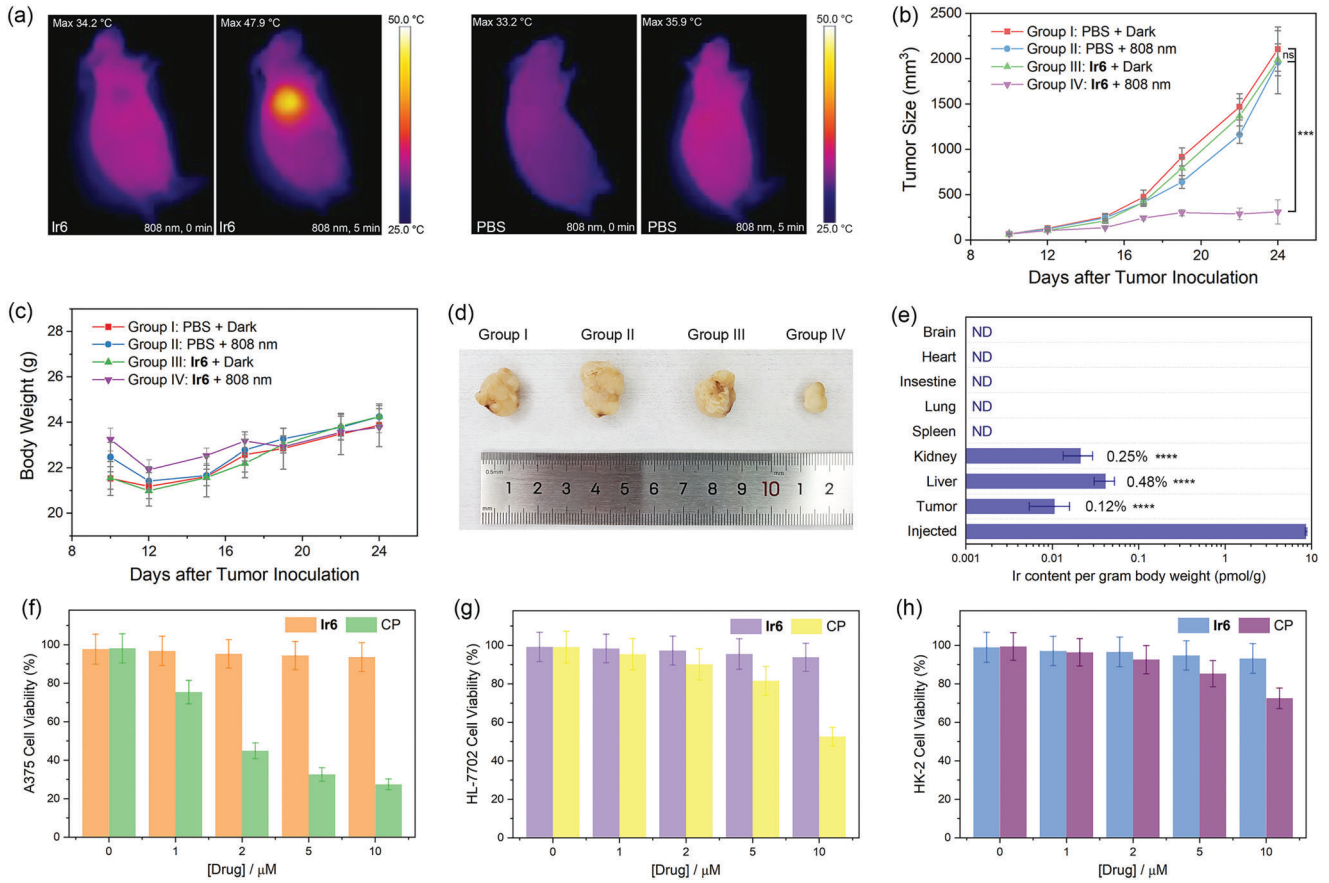

Figure 4. In vivo dual PDT/PTT assay and hepato-/nephrotoxicity evaluation of **Ir6**. a) Real-time thermal images of BALB/c nude mice (subcutaneous A375 human melanoma xenograft model) before and after the in vivo dual PDT/PTT assay ($n = 5$). b) Tumor growth curves of the four groups after various treatments ($n = 5$). c) Body weight curves of the four groups after various treatments ($n = 5$). d) Photograph of representative post-treatment solid tumors for each group ($n = 5$). e) Iridium amounts in the collected organs in **Ir6**-injected groups (Group III and IV, 14 d after injection, $n = 5$). ND: not detected. The amount of iridium administered was calculated by the total body weight. Cell viability of f) human malignant melanoma cell line A375, g) human normal liver cell line HL-7702, and h) human normal kidney cell line HK-2 incubated with various dose of **Ir6** and cisplatin (CP) for 24 h ([drug] = 0–10 × 10^{-6} M). Data represent the mean ± SD ($n = 6$).

2.11. In Vivo Dual PDT/PTT

A375 tumor-bearing mice (BALB/c mouse model with tumor xenografts) of different drug groups were intratumorally injected with **Ir6**, irradiated with 808 nm LPL (Group IV, 0.1 W cm^{-2}, light dose = 30.0 J cm^{-2}) or untreated (Group III). The control groups received PBS injections and were handled both with and without irradiation (Group II and I). The body temperatures of mice were tracked by IR thermal images. After irradiation, the temperature of tumor sites in mice (Group IV) rose to 47.9 °C (ΔT = 13.7 °C, **Figure 4**a), while ΔT values in the other groups were <1.0 °C. A temperature exceeding 41 °C is considered effective for destroying tumor tissue.[28] No skin injury occurred during phototherapy, since the irradiation of 808 nm LPL in this study was below 30% of the MPE standard for laser exposure to skin (0.33 W cm^{-2}). After 14 d, the tumor mean volume (V) of Groups I–III reached 2000 mm^3 (Figure 4b), and there was no loss of body weight in the mice (Figure 4c), indicating that the systemic toxicity of **Ir6** in mice without irradiation is extremely low. The irradiation group (Group IV) showed a substantial antitumor effect with a value of 310 mm^3 and an inhibition rate of 85% (Figure 4d). The different hematoxylin and eosin (H&E) staining pattern of Group IV tumor sections compared to the others suggests that **Ir6**-mediated dual PDT/PTT can cause damage to tumor tissues, whereas no appreciable lesions were observed in the H&E staining of sections from the major organs (Figure S14, Supporting Information), confirming the nontoxic nature of **Ir6** in vivo.

2.12. Biodistribution and Hepato-/Nephrotoxicity Evaluation

The toxicity of heavy metals to the human body, particularly hepatotoxicity and nephrotoxicity, is a major safety concern for metal-containing drugs. While studies have focused on the effectiveness of drug distribution to tumors over hours after injection into animals, residues and potential toxicity after treatment have been largely overlooked. Here, we used ICP-MS to analyze the amount of Ir residues in the collected organs and tumors (Figure 4e) from the **Ir6**-injected mice at the end of the in vivo assay (14 d after administration). Unsurprisingly, trace quantities of Ir were detected in tumors, kidneys, and livers, but none in other organs. **Ir6** can be cleared from the body more efficiently than cisplatin

($t_{1/2}$ = 58–73 h), Porfimer Sodium ($t_{1/2}$ = 250 h), and Photofrin II ($t_{1/2}$ > 100 h), as shown by the mean total residue of 0.85% in ten **Ir6**-injected mice (estimated $t_{1/2}$ = 48 h). A short half-life is also beneficial for the rapid excretion of the PS following phototherapy to reduce side effects such as photodermatosis.

In order to verify whether the residue is toxic to the liver and kidney, the cytotoxicities of **Ir6** and cisplatin to human normal liver (HL-7702) and kidney (HK-2) cells have been further studied. In vitro cytotoxicity studies have demonstrated that **Ir6** has minimal cytotoxicity to A375 cells in the absence of irradiation, whereas cisplatin can significantly inhibit the growth of A375 cells (Figure 4f). In the case of HL-7702 and HK-2 cells, cisplatin also exhibited similar toxicity. In contrast, **Ir6** was much less toxic to these two normal cells. At concentrations of 1–10 × 10^{-6} M, which is 5–6 orders of magnitude higher than the total residue of Ir6 in mice, normal cell viability remained greater than 99% to 93% (Figure 4g,h). This allows **Ir6** to reach a level of relative safety prior to its total removal from the body.

3. Conclusions

In conclusion, by rational design and distribution of excited state energy, a series of single-molecule Ir(III) complexes have been endowed with the capability to act as infrared two-photon absorption, dual PDT and PTT reagents using an 808 nm low-power laser. **Ir6**, the most potent complex in the series, has exhibited a remarkable phototherapy index in vitro and dual PDT and PTT activity for malignant melanoma in vivo. **Ir6** also has minimal hepato-/nephrotoxicity in vitro and can be eliminated from the body effectively. These findings may contribute to the development of highly efficient phototherapeutic drugs for large, deeply buried solid tumors in hypoxic environments.

4. Experimental Section

The details of the experimental section including materials, instruments, synthesis, characterization, DFT calculations, singlet oxygen quantum yield, lipophilicity (log $K_{o/w}$), photothermal conversion efficiency, subcellular colocalization, cell uptake, in vitro cytotoxicity, flow cytometry analysis, caspase activation, and in vivo dual PDT/PTT therapy are given in the Supporting Information. All animal experiments were reviewed and approved by the Institutional Animal Care and Use Committee (IACUC) at Yunnan University, Kunming, China (Approval No. YNU20220269). Dr. Xiaoxia Ren (Laboratory Animal Certificate 1118062800091) at Animal Research and Resource Center (accreditation number SYXK (滇) K2021-0002), Yunnan University, Kunming, China, performed the experiments and collected the data.

Statistical Analysis: At least three replicates were performed for the experiments, and the data were presented as mean ± standard deviation (SD). Significance difference between two groups was assessed by unpaired Student's test (two-sided) using Origin 9.0 software. The sample sizes (n) for each statistical analysis were as follows: cytotoxicity (n = 6), mouse bodyweight (n = 5), tumor size (n = 5). $P < 0.05$ was the accepted level of significance.

Supporting Information

Supporting Information is available from the Wiley Online Library or from the author.

Acknowledgements

S.-J.T. and Q.-F.L. contributed equally to this work. This work was supported by the National Natural Science Foundation of China (22167022), Yunnan Provincial Science and Technology Department (2018FB022), and Youth Talents Project of Yunnan Province (2018-057). The authors thank the Advanced Analysis and Measurement Center of Yunnan University for their help in characterization.

Conflict of Interest

The authors declare no conflict of interest.

Data Availability Statement

The data that support the findings of this study are available from the corresponding author upon reasonable request.

Keywords

antitumor therapy, iridium complexes, photodynamic therapy, photothermal therapy

Received: April 26, 2023
Revised: May 30, 2023
Published online: June 20, 2023

[1] a) L. Zhang, N. Montesdeoca, J. Karges, H. Xiao, *Angew. Chem., Int. Ed.* **2023**, *62*, e202300662; b) S. Sen, M. Won, M. S. Levine, Y. Noh, A. C. Sedgwick, J. S. Kim, J. L. Sessler, J. F. Arambula, *Chem. Soc. Rev.* **2022**, *51*, 1212; c) J. Karges, *Angew. Chem., Int. Ed.* **2022**, *61*, e202112236.
[2] a) Z. S. Yang, Y. H. Yao, A. C. Sedgwick, C. C. Li, Y. Xia, Y. Wang, L. Kang, H. M. Su, B. W. Wang, S. Gao, J. L. Sessler, J. L. Zhang, *Chem. Sci.* **2020**, *11*, 8204; b) J. Du, T. Shi, S. Long, P. Chen, W. Sun, J. Fan, X. Peng, *Coord. Chem. Rev.* **2021**, *427*, 213604.
[3] X. Li, J. F. Lovell, J. Yoon, X. Chen, *Nat. Rev. Clin. Oncol.* **2020**, *17*, 657.
[4] a) L. P. Zhang, Y. Geng, L. J. Li, X. F. Tong, S. Liu, X. M. Liu, Z. M. Su, Z. G. Xie, D. X. Zhu, M. R. Bryce, *Chem. Sci.* **2021**, *12*, 5918; b) B. Liu, J. Jiao, W. Xu, M. Zhang, P. Cui, Z. Guo, Y. Deng, H. Chen, W. Sun, *Adv. Mater.* **2021**, *33*, 2100795; c) J. Zhao, K. Yan, G. Xu, X. Liu, Q. Zhao, C. Xu, S. Gou, *Adv. Funct. Mater.* **2020**, *31*, 2008325.
[5] T. C. Pham, V. N. Nguyen, Y. Choi, S. Lee, J. Yoon, *Chem. Rev.* **2021**, *121*, 13454.
[6] M.-F. Wang, R. Yang, S.-J. Tang, Y.-A. Deng, G.-K. Li, D. Zhang, D. Chen, X. Ren, F. Gao, *Angew. Chem., Int. Ed.* **2022**, *61*, e202208721.
[7] M.-F. Wang, Y.-A. Deng, Q.-F. Li, S.-J. Tang, R. Yang, R.-Y. Zhao, F.-D. Liu, X. Ren, D. Zhang, F. Gao, *Chem. Commun.* **2022**, *58*, 12676.
[8] a) H. Madec, F. Figueiredo, K. Cariou, S. Roland, M. Sollogoub, G. Gasser, *Chem. Sci.* **2023**, *14*, 409; b) Z. Ma, H. Han, Y. Zhao, *Biomaterials* **2023**, *293*, 121947; c) B. Kar, U. Das, N. Roy, P. Paira, *Coord. Chem. Rev.* **2023**, *474*, 214860; d) L. C.-C. Lee, K. K.-W. Lo, *J. Am. Chem. Soc.* **2022**, *144*, 14420.
[9] L. A. Ortiz-Rodríguez, C. E. Crespo-Hernández, *Chem. Sci.* **2020**, *11*, 11113.
[10] Z. Lv, H. Wei, Q. Li, X. Su, S. Liu, K. Y. Zhang, W. Lv, Q. Zhao, X. Li, W. Huang, *Chem. Sci.* **2018**, *9*, 502.
[11] a) B. Liu, L. Lystrom, S. Kilina, W. Sun, *Inorg. Chem.* **2019**, *58*, 476; b) X.-D. Bi, R. Yang, Y.-C. Zhou, D. Chen, G.-K. Li, Y.-X. Guo, M.-F. Wang, D. Liu, F. Gao, *Inorg. Chem.* **2020**, *59*, 14920.

[12] A. Colombo, C. Dragonetti, D. Roberto, A. Valore, C. Ferrante, I. Fortunati, A. L. Picone, F. Todescato, J. A. G. Williams, *Dalton Trans.* **2015**, *44*, 15712.
[13] a) H. Wang, X. Tian, L. Guan, Q. Zhang, S. Zhang, H. Zhou, J. Wu, Y. Tian, *J. Mater. Chem. B* **2016**, *4*, 2895; b) Q. Zhang, X. Tian, H. Zhou, J. Wu, Y. Tian, *Materials* **2017**, *10*, 223.
[14] W. J. Xu, S. J. Liu, X. Zhao, N. Zhao, Z. Q. Liu, H. Xu, H. Liang, Q. Zhao, X. Q. Yu, W. Huang, *Chem. - Eur. J.* **2013**, *19*, 621.
[15] P. Hanczyc, B. Norden, M. Samoc, *Dalton Trans.* **2012**, *41*, 3123.
[16] a) D. An, J. Fu, B. Zhang, N. Xie, G. Nie, H. Ågren, M. Qiu, H. Zhang, *Adv. Funct. Mater.* **2021**, *31*, 2101625; b) H. Li, H. Wen, Z. Zhang, N. Song, R. T. K. Kwok, J. W. Y. Lam, L. Wang, D. Wang, B. Z. Tang, *Angew. Chem., Int. Ed.* **2020**, *59*, 20371; c) Z. Yu, W. K. Chan, Y. Zhang, T. T. Y. Tan, *Biomaterials* **2021**, *269*, 120459.
[17] a) D. Xi, M. Xiao, J. Cao, L. Zhao, N. Xu, S. Long, J. Fan, K. Shao, W. Sun, X. Yan, X. Peng, *Adv. Mater.* **2020**, *32*, 1907855; b) H. S. Jung, P. Verwilst, A. Sharma, J. Shin, J. L. Sessler, J. S. Kim, *Chem. Soc. Rev.* **2018**, *47*, 2280.
[18] M. Stocks, in *Introduction to Biological and Small Molecule Drug Research and Development* (Eds.: R. Ganellin, S. Roberts, R. Jefferis), Elsevier, Oxford **2013**, pp. 81–126.
[19] I. N. Novikova, E. V. Potapova, V. V. Dremin, A. V. Dunaev, A. Y. Abramov, *Life Sci.* **2022**, *304*, 120720.
[20] S. P. Cullen, S. J. Martin, *Cell Death Differ.* **2009**, *16*, 935.
[21] M. Pérez-Hernández, P. del Pino, S. G. Mitchell, M. Moros, G. Stepien, B. Pelaz, W. J. Parak, E. M. Gálvez, J. Pardo, J. M. de la Fuente, *ACS Nano* **2015**, *9*, 52.